PROTEINS: Structure, Function, and Bioinformatics 60:181–186 (2005)

CAPRI Rounds 3–5 Reveal Promising Successes and Future Challenges for RosettaDock

Michael D. Daily,[1] David Masica,[1] Arvind Sivasubramanian,[2] Sony Somarouthu,[2] and Jeffrey J. Gray[1,2]*
[1]*Program in Molecular Biophysics, Johns Hopkins University, Baltimore, Maryland*
[2]*Department of Chemical and Biomolecular Engineering, Johns Hopkins University, Baltimore, Maryland*

ABSTRACT **CAPRI Rounds 3, 4, and 5 are the first public test of the published RosettaDock algorithm. The targets cover a wide range of sizes and shapes. For most targets, published biological information indicated the region of the binding site on at least one docking partner. The RosettaDock algorithm produced high accuracy predictions for three targets, medium-accuracy predictions for two targets, and an acceptable prediction for one target. RosettaDock predicted all five targets with less than 450 residues to high or medium accuracy, but it predicted only one of seven targets with above 450 residues to acceptable accuracy. RosettaDock's high-accuracy predictions for small to moderately large targets reveal the predictive power and fidelity of the algorithm, especially the high-resolution refinement and scoring protocol. In addition, RosettaDock can predict complexes from at least one homology-modeled docking partner with comparable accuracy to unbound cases of similar size. Larger targets present a more intensive sampling problem, and some large targets present repulsive barriers to entering the binding site. Ongoing improvements to RosettaDock's low-resolution search may alleviate this problem. This first public test suggests that RosettaDock can be useful in a significant range of applications in biochemistry and cell biology. Proteins 2005;60:181–186.**

Key words: protein–protein docking; RosettaDock; Rosetta; CAPRI; biomolecular modeling; protein structure prediction; homology or comparative modeling

INTRODUCTION

Protein–protein docking is one of the major unsolved problems of biochemistry and cell biology today. Protein–protein interactions are integral to many mechanisms of cellular control, including protein localization, competitive inhibition, allosteric regulation, gene regulation, and signal transduction. Disruption of protein–protein interactions can cause biochemical diseases related to these functions. The prediction of protein–protein interactions, if it is accurate and consistent enough, can greatly increase the amount of structural information available to understand the function of biologically important complexes.

Protein–protein docking is energetically governed by desolvation, van der Waals interactions, electrostatics, and favorable specific interactions like hydrogen bonds. In addition, amino acid side-chains at the interface must attain favorable conformations. Protein docking algorithms must sample over an immense translational, rotational, and conformational search space and score the many components of the protein interaction energy with high accuracy and sensitivity. Multiple protein docking algorithms have been developed, and most use a Fast Fourier Transform (FFT) algorithm that rapidly samples possible interactions in a grid representation with a simple energy function comprising shape complimentarity, electrostatics, and/or desolvation. Some algorithms refine the structures after FFT. Instead of a grid-based search, the RosettaDock algorithm[1] uses a low-resolution (recognition) Monte Carlo search, which mimics the natural diffusion process, followed by all-atom refinement, including side-chain refinement, to account for possible side-chain conformational changes upon binding.

Testing of docking algorithms in recent years has revealed mixed results. Chen et al. recently published a docking benchmark set of 52 targets.[2] Vajda and Camacho analyzed the performance of three docking algorithms on this benchmark.[3] All algorithms correctly predict most targets with apolar interfaces and/or large interface areas, but polar interfaces are accurately predicted less often, and small signaling proteins are often inaccurately predicted. RosettaDock predicts polar interfaces more consistently than other algorithms, although its overall performance is similar to that of other algorithms. This suggests that current docking algorithms have successfully captured the basic biophysical principles behind protein–protein interactions. However, an algorithm that can correctly predict the diverse types of interactions that exist in nature is still probably several years away.

CAPRI is a blind, publicly verifiable test of protein–protein docking algorithms.[4] Targets are predicted prior to publication of the coordinates of the complex. The targets of CAPRI Rounds 3–5 present a broad range of complex types, including enzyme–inhibitor and antibody–antigen

Grant sponsor: National Institutes of Health; Grant number: K01-HG002316 (to Jeffrey J. Gray). Grant sponsor: ARCS Foundation Fellowship (to Michael D. Daily).

*Correspondence to: Jeffrey J. Gray, Program in Molecular Biophysics and Department of Biomolecular Engineering, Johns Hopkins University, 3400 N. Charles Street, Baltimore, MD 21218. E-mail: jgray@jhu.edu

Received 11 January 2005; Accepted 31 January 2005

DOI: 10.1002/prot.20555

TABLE I. Evaluation Statistics of CAPRI Targets 8–19

Target	Complex	Type[b]	N_{res}	Model	F_{nat}	Lrms (Å)	Irms (Å)	Accuracy[d]
15[a]	Colicin D—immD	BB-BB	194	7	0.88	0.547	0.243	***
12	Cohesin–dockerin	U-B	196	1	0.87	0.99	0.51	***
11	Cohesin–dockerin	U-H	196	5	0.42	6.11	1.17	**
19	Prion–Fab	H-B	312[c]	2	0.64	3.64	1.27	**
8	Laminin–nidogen	U-B	427	2	0.53	4.63	0.66	***
17[a]	GH11 xylanase–XIP	H-U	464	5	0.07	12.91	8.78	—
13	SAG1–Fab	U-B	474[c]	NP	NP	NP	NP	—
18	GH11 xylanase–TAXI	U-B	552	NP	NP	NP	NP	—
16[a]	GH10 xylanase–XIP	H-U	575	7	0.14	8.13	11.64	*
14	MYPT1–PP1	U-B	600	NP	NP	NP	NP	—

[a]Officially canceled by the CAPRI evaluation committee.
[b]U: unbound; B: bound; H: homology model; BB: bound backbone.
[c]Size with antigen + only F_v domains of antibody.
[d]Star rankings correspond with ranking criteria of Méndez et al.[13]
Abbreviations: N_{res}: number of residues in complex; F_{nat}: fraction of native contacts; Lrms: RMSD of smaller partner; Irms: RMSD of interface residues; NP: not predicted.
Targets 11, 19, 17, and 16 were predicted with one homology-modeled docking partner.

targets, and sizes ranging from under 200 to over 1100 total residues. In four targets of Rounds 4 and 5, one or more of the monomers had to be built from a template of at least 50% sequence identity. The homology docking challenge is well suited for the Rosetta protein modeling suite,[5] which can perform both comparative modeling[6,7] and docking.[1]

RosettaDock submitted predictions for 10 of 12 targets in Rounds 3–5 and 6 of these 10 targets were predicted to acceptable or better accuracy, including three high-accuracy predictions. The successful predictions reveal key strengths of RosettaDock, like side-chain refinement and high-resolution scoring, but the unsuccessful predictions show how complicated challenges like large complex sizes and interwoven interfaces can frustrate RosettaDock.

MATERIALS AND METHODS

The RosettaDock algorithm[1] models physical forces when possible, but energy terms are parameterized using data from high-resolution protein structures rather than small molecules, as in traditional molecular mechanics approaches. RosettaDock also refines structures to be consistent with high-resolution structural and energetic patterns of known complexes. The sampling problem is attacked with supercomputing clusters to create very large numbers of decoys. Residue-scale potentials are used to enable faster computation and to average interactions over long length and timescales during the initial search of conformational space. Physically based all-atom potentials are then used for refinement of decoys and accurate discrimination. Finally, algorithm convergence, as measured by solution degeneracy after decoy clustering, is used as a final criterion in decoy selection.

The algorithm first uses a fast low-resolution, rigid-body Monte Carlo search with residue-scale potentials. This process mimics the steps involved in a diffusional encounter between two macromolecules. The finished low-resolution decoy then undergoes simultaneous atomic-scale optimization of rigid-body displacement and side-chain conformations using Monte Carlo sampling plus minimization.[8] Simultaneous optimization is very important, because the final rigid-body position depends on the final conformations of side chains and vice versa. RosettaDock refines side chains by the protocol of Kuhlman and Baker,[9] which uses a simulated annealing search through backbone-dependent rotamers,[10] varying all χ angles over the library positions supplemented with χ_1 rotamer angles plus and minus one standard deviation from the respective means. Up to 5×10^5 independent simulations are carried out, and the resulting decoys are ranked using an energy function that is dominated by van der Waals interactions, an implicit solvation model,[11] and an orientation-dependent hydrogen bonding potential.[12] Ranked decoys are then clustered with a 2.5 Å root-mean-square distance (RMSD) cutoff to identify the most entropically accessible minima and to limit the effect of inaccuracies in the potential function. Decoy clusters are ranked for submission by cluster size and score, but they are carefully visually examined for close packing and consistency with known biochemical information. Any model with poor packing, a small interface, and/or a high radius of gyration is discarded from the submission set.

A detailed description of RosettaDock, including the search strategy and the parameterization of the scoring functions, has been published.[1] The RosettaDock source code and user documentation are available at http://graylab.jhu.edu.

TARGETS AND PREDICTIONS

Table I shows our results for the targets of CAPRI Rounds 3, 4, and 5. RosettaDock predicted three targets to high accuracy, two to medium accuracy, and one to acceptable accuracy according to the criteria used by Méndez et al.[13] in the first two rounds of CAPRI. RosettaDock predicted four others incorrectly, and we did not participate in the challenge for Targets 9 and 10. We include our

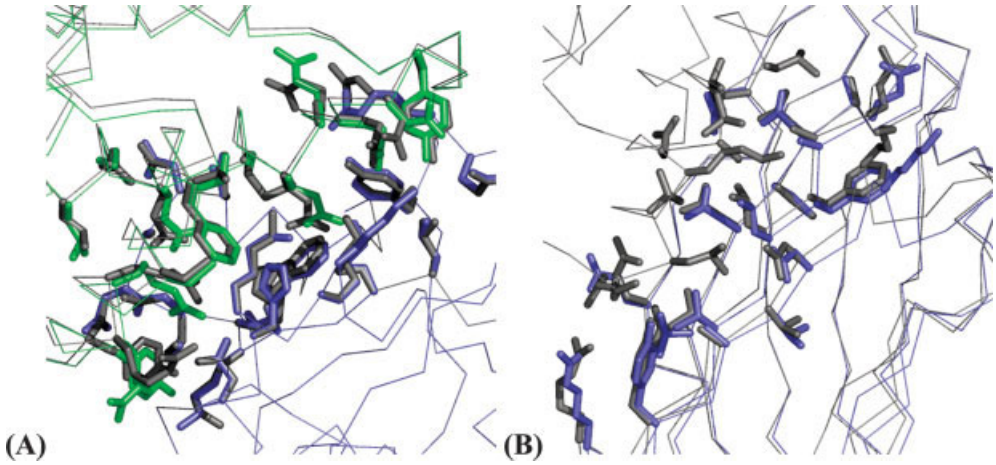

Fig. 1. RosettaDock predictions with atomic accuracy in side chains. (**A**) T15: Colicin D–immD. Gray: native structure[15]; blue: predicted Colicin D; green: predicted ImmD. 88% contacts, 0.55 Å Lrms, 0.24 Å Irms, 75% correct interface side-chain conformations. (**B**) T12: Cohesin–dockerin. Gray: native structure[18]; blue: predicted cohesin. 87% contacts, 0.99 Å Lrms, 0.51 Å Irms, 67% correct interface side-chain conformations.

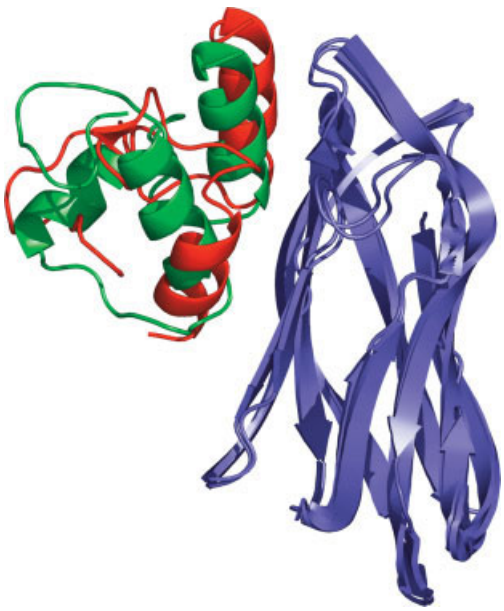

Fig. 2. Homology docking prediction in CAPRI. T11: Cohesin–dockerin. Blue: cohesin; red: predicted dockerin homology model; green: native dockerin.[18] 42% contacts, 6.11 Å Lrms, 1.17 Å Irms.

Fig. 3. High-accuracy prediction of T8 using 759–848 fragment of laminin. T8: Laminin–nidogen. Blue: nidogen; red: predicted laminin (759–848 fragment); green: native laminin.[23] 53% contacts, 4.63 Å Lrms, 0.66 Å Irms.

results for the canceled targets 15–17, all of which we submitted before we were notified that there was any public information about the coordinates.

Target 15: Colicin D–ImmD

Colicin D mutant H611Y is catalytically inactive,[14] so we hypothesized that H611 should be at the interface. Because bound structures of colicin D and ImmD without side chains were provided, the side chains were generated during docking using rotamer packing. Ten of fifteen models obtained by clustering the top 200 of 500,000 decoys were selected for submission based upon close packing and the presence of H611 at the interface. Model 7 [Fig. 1(A)] had 88% of native contacts, 0.54 Å RMSD, and 0.24 Å interface RMSD from the crystal structure,[15] and 75% of interface residues were predicted in the correct side-chain conformation, which is RosettaDock's most accurate CAPRI prediction ever by all four criteria.

Target 12: Cohesin–Dockerin

Dockerin residues 11, 12, 45, and 46 control the specificity of the cohesin–dockerin interaction,[16] so helices 1 and 3 of dockerin were preoriented toward cohesin. Furthermore, the 8,3,6,5 face of the cohesin β-jelly roll had been hypothesized to interact with dockerin because it is the more conserved face.[17] Four models were predicted by docking unbound cohesin to bound dockerin, and these models were submitted in rank order by score. Model 1 [Fig. 1(B)] had 87% of native contacts, 0.99 Å RMSD, and 0.51 Å interface RMSD from the crystal structure,[18] and 67% of interface residues were predicted in the correct side-chain conformation. Figure 1 shows the atomic-level accuracy of interface predictions for T15 and T12.

Target 11: Cohesin–Homology-Modeled Dockerin

A model of dockerin was constructed from the minimized, average NMR structure of a 52% identical dockerin[19] using the Robetta homology-modeling server.[7] Dockerin was preoriented toward cohesin, as with Target 12. Models were ranked based on close packing and presence of dockerin residues 11, 12, 45, and 46, and the cohesin β-8,3,6,5 face at the interface. Model 6 (Fig. 2) had 42% native contacts, 6.11 Å RMSD, and 1.17 Å interface RMSD from the crystal structure.[18] The rigid-body position of dockerin is surprisingly accurate given the significant backbone deviations in the homology-modeled dockerin.

Target 19: Prion–Antibody Fragment (Fab)

The NMR structure of a 95% identical prion[20] and the bound coordinates of the Fab were provided. The five differing side-chains of the prion were replaced in the minimized average NMR structure by rotamer packing during docking. The Fab coordinates were reduced to the F_v domains, the Fab complementarity determining regions (CDRs) were preoriented toward the prion, and docking to the Fab was constrained to the CDRs using RosettaDock antibody constraints.[1] The top 1000 of 10^5 decoys were clustered, and the largest 10 clusters were submitted in rank order by cluster size. Model 2 had 64% native contacts, 3.64 Å RMSD, and 1.27 Å interface RMSD from the crystal structure.[21]

Target 8: Laminin–Nidogen

Residues D800, N802, and V804 in laminin module LE4 are required to form the laminin-nidogen complex.[22] Three fragments of laminin were independently docked to nidogen: all of laminin, module LE4 (residues 793–848), and part of module LE3 plus module LE4 (residues 759–848). We chose the 759–848 fragment because it contained the 800–804 loop in the center, and it was as long as the entire width of nidogen. For all docking runs, the laminin 800–804 loop was preoriented toward nidogen, and models were selected and ranked for submission based on close packing and the presence of the 800–804 loop at the interface. Six models from the fragment 793–848 run, two models from the fragment 759–848 run, and two models containing all of laminin were submitted. Submitted model 2 (Fig. 3), from the 759–848 fragment, had 53% native contacts, 4.63 Å RMSD, and 0.66 Å interface RMSD from the crystal structure,[23] which was the best T8 prediction by ligand RMSD.

Target 17: Family 11 Xylanase–XIP-1 Xylanase Inhibitor

Penicillium funiculosum xylanase was built from the 60% identical *Trichoderma reesei* xylanase structure[24] using Robetta.[7] The known family 11 xylanase active site and the nearby binding-critical thumb region[25] were preoriented toward XIP-1. Ten models were selected and ranked for submission based on closeness of packing and presence of the xylanase thumb at the interface. Model 5 contained the correct binding region but with a significant xylanase rotation compared to the crystal structure.[26] In a score versus RMSD plot (binding funnel) constructed from a small perturbation run on the crystal structure of T17, the native structure scores well, but there is limited sampling nearby; that is, there is a significant repulsion barrier blocking the active site.

Target 13: SAG1 Antigen–Fab Complex

The SAG1 antigen comprises two β-jelly roll domains, domain D1 (residues 1–131) and domain D2 (residues 132–255). Three fragments of SAG1 were docked independently to the Fab: all of SAG1, domain D1 only, and domain D2 only. For all docking runs, the Fab was truncated to the F_v domains, the Fab CDRs were preoriented toward SAG1, and docking to the Fab was constrained to the CDRs, as with T19. Because SAG1 domain D2 contains an epitope for immune response to SAG1 in mice,[27] the top six D2 models, the top three D1 models, and one whole SAG1 model were submitted. No submitted models were correct, but D1 model 5 was 2.95 Å RMSD from the crystal structure, and 73% of interface side-chains were predicted in the correct conformation. The mouse epitope does not interact with the Fab, and we should have disregarded this epitope because it was not specific to the T13 complex.

Target 18: Family 11 Xylanase–TAXI-1

The known family 11 xylanase active site and thumb regions[25] were preoriented toward the inhibitor. No correct models were predicted for T18. In a binding funnel constructed from a perturbation run on the crystal structure of T18,[28] there is slightly restricted sampling around the native position, which implies a slight steric hindrance to accessing the binding site.

Target 16: Family 10 Xylanase–XIP-1 Xylanase Inhibitor

Aspergillus nidulans xylanase, a family 10 xylanase, was built from the 66% identical *Penicillium simplicissimum* xylanase structure[29] using Robetta,[7] and the known family 10 xylanase active site[29] was preoriented toward XIP-1. Models were selected and ranked for submission based on closeness of packing and degree of blockage of the active site of xylanase. Model 7 had 14% of native contacts, 8.13 Å RMSD, and 11.64 Å interface RMSD. While XIP-1 bound to xylanase with some rigid-body rotation from the crystal structure,[26] this model is an admirable prediction given the large size of T16.

Target 14: Protein Phosphatase-1 (PP1)–MYPT1

Large, multidomain MYPT1 was divided into the N-terminal peptide (residues 1–39) and the two ankyrin repeat domains (residues 40–164 and 165–291). Each fragment was docked independently to PP1, and then the rest of MYPT1 was superimposed onto the predicted fragment position. In one prediction for ankyrin domain 40–164, when the rest of MYPT1 was superimposed, domain 165–291 fit PP1 closely with few clashes, but the N-terminal peptide did not contact PP1. The superimposed model was optimized to remove clashes, and several

models from this perturbation plus a few superimposed, optimized models from the ankyrin domain 165–291 starting structure were submitted. No models were close to the crystal structure,[30] which has a smaller and more extended interface than we expected.

DISCUSSION

The 10 CAPRI targets for which we submitted models tested the predictive power of RosettaDock over a broad variety of protein complex shapes, sizes, and interface types. RosettaDock produced medium to high accuracy predictions for five easy-to-moderately difficult targets, but RosettaDock was confounded by five other targets, with complications like large sizes and/or interwoven interfaces.

Targets 15, 12, 11, 19, and 8, for which RosettaDock produced medium or high accuracy predictions, are less than 450 total residues, and none of them has a repulsive barrier to entering the binding site. RosettaDock's best predictions, T15 and T12 (Fig. 1), are highly accurate by side-chain conformation as well as by contacts, RMSD, and interface RMSD. The T15 prediction has 75% correct interface rotamers, and the T12 prediction has 67% correct interface rotamers. RosettaDock overcame the 427-residue size of T8 to produce a high-accuracy prediction by docking only the portions of laminin known to interact with nidogen.

RosettaDock predicted homology docking targets 11 and 19 to medium accuracy, and it predicted target 16 to acceptable accuracy, which demonstrates that the algorithm can accurately predict rigid-body position in spite of small conformational inaccuracies in a starting structure. RosettaDock's predictions for these homology docking targets also show that Rosetta can effectively integrate its independently successful homology modeling[31] and docking[1,32] functions into a multistage biomolecular modeling package.

RosettaDock's successful predictions for these five targets reveal the power and accuracy of its side-chain packing and refinement algorithm and detailed scoring function. Side-chain prediction contributed to high accuracy rigid-body predictions for T15 and T12, and RosettaDock predicted three other targets to medium or better accuracy even though these targets had only 7–33% of interface side chains in the correct conformation. For all five medium or better predictions, RosettaDock ranked the correct prediction among the top 10 scoring clusters, but it ranked the correct prediction as the top model in only one target. This demonstrates that the scoring function works well but not perfectly. The scoring function provides accurate discrimination by taking into account not only basic properties like van der Waals interactions and desolvation, but also the details of side-chain packing and hydrogen bonding.

Targets 17, 13, 18, 16, and 14 present additional challenges that hamper the predictive power of RosettaDock. All of these targets are larger than 450 residues. In T13, SAG1 contained two domains, either of which could have bound to the Fab, which made model selection difficult. In T17 and T18, narrow active site grooves hindered inhibitor binding to xylanase, and in T14, the long N-terminal helical arm of MYPT1 made it difficult for PP1 to bind MYPT1. Partially blocked binding funnels for T17 and T18 support this hypothesis. RosettaDock overcame the limitation of size in one case by predicting an acceptable model for 575-residue T16.

Limitations in our low-resolution (recognition) search may have contributed to incorrect predictions for four large targets. We are currently developing a more sensitive residue-scale contact potential to improve shape complimentarity recognition. In addition, FFT-based methods, which can directly sample all possible configurations without entry barriers, successfully predicted T18 and T14, which Monte Carlo-based RosettaDock failed to predict. (Schueler-Furman and coworkers[33] successfully predicted sterically hindered T14, but only by breaking MYPT1 into domains before docking. Probably only an FFT method could have correctly predicted T14 with full-length MYPT1 as a starting structure.) Better predictions might be obtained in future rounds of CAPRI by integrating an FFT-based low-resolution search with RosettaDock's successful high-resolution refinement and scoring.

In most CAPRI targets, we constrained docking beforehand and more easily selected correct models in postprocessing by using biological information. The crystal structures of the targets were always consistent with specific biological information like binding-critical mutants and active site residues.

This first blind public test of the RosettaDock algorithm suggests that the method will be useful in a significant range of biological applications.

ACKNOWLDEGMENTS

We thankfully acknowledge the efforts of the CAPRI organizers in finding and evaluating targets and facilitating communication between protein docking groups. We are also grateful to the crystallographers for offering their complexes as CAPRI targets to challenge the performance of our algorithm.

REFERENCES

1. Gray JJ, Moughon S, Wang C, Schueler-Furman O, Kuhlman B, Rohl CA, Baker D. Protein–protein docking with simultaneous optimization of rigid-body displacement and side-chain conformations. J Mol Biol 2003;331:281–299.
2. Chen R, Mintseris J, Janin J, Weng Z. A protein–protein docking benchmark. Proteins 2003;52:88–91.
3. Vajda S, Camacho CJ. Protein–protein docking: is the glass half-full or half-empty? Trends Biotechnol 2004;22:110–116.
4. Janin J, Henrick K, Moult J, Eyck LT, Sternberg MJ, Vajda S, Vakser I, Wodak SJ. CAPRI: a Critical Assessment of PRedicted Interactions. Proteins 2003;52:2–9.
5. Rohl CA, Strauss CE, Misura KM, Baker D. Protein structure prediction using Rosetta. Methods Enzymol 2004;383:66–93.
6. Rohl CA, Strauss CE, Chivian D, Baker D. Modeling structurally variable regions in homologous proteins with Rosetta. Proteins 2004;55:656–677.
7. Chivian D, Kim DE, Malmstrom L, Bradley P, Robertson T, Murphy P, Strauss CE, Bonneau R, Rohl CA, Baker D. Automated prediction of CASP-5 structures using the Robetta server. Proteins 2003;53(Suppl 6):524–533.
8. Li Z, Scheraga HA. Monte Carlo–minimization approach to the multiple-minima problem in protein folding. Proc Natl Acad Sci USA 1987;84:6611–6615.

9. Kuhlman B, Baker D. Native protein sequences are close to optimal for their structures. Proc Natl Acad Sci USA 2000;97: 10383–10388.
10. Dunbrack RL Jr, Cohen FE. Bayesian statistical analysis of protein side-chain rotamer preferences. Protein Sci 1997;6:1661–1681.
11. Lazaridis T, Karplus M. Effective energy function for proteins in solution. Proteins 1999;35:133–152.
12. Kortemme T, Morozov AV, Baker D. An orientation-dependent hydrogen bonding potential improves prediction of specificity and structure for proteins and protein–protein complexes. J Mol Biol 2003;326:1239–1259.
13. Méndez R, Leplae R, De Maria L, Wodak SJ. Assessment of blind predictions of protein–protein interactions: current status of docking methods. Proteins 2003;52:51–67.
14. Tomita K, Ogawa T, Uozumi T, Watanabe K, Masaki H. A cytotoxic ribonuclease which specifically cleaves four isoaccepting arginine tRNAs at their anticodon loops. Proc Natl Acad Sci USA 2000;97:8278–8283.
15. Graille M, Mora L, Buckingham RH, Van Tilbeurgh H, De Zamaroczy M. Structural inhibition of the colicin D tRNase by the tRNA-mimicking immunity protein. EMBO J 2004;23:1474–1482.
16. Mechaly A, Yaron S, Lamed R, Fierobe HP, Belaich A, Belaich JP, Shoham Y, Bayer EA. Cohesin-dockerin recognition in cellulosome assembly: experiment versus hypothesis. Proteins 2000;39: 170–177.
17. Shimon LJ, Bayer EA, Morag E, Lamed R, Yaron S, Shoham Y, Frolow F. A cohesin domain from *Clostridium thermocellum*: the crystal structure provides new insights into cellulosome assembly. Structure 1997;5:381–390.
18. Carvalho AL, Dias FM, Prates JA, Nagy T, Gilbert HJ, Davies GJ, Ferreira LM, Romao MJ, Fontes CM. Cellulosome assembly revealed by the crystal structure of the cohesin-dockerin complex. Proc Natl Acad Sci USA 2003;100:13809–13814.
19. Lytle BL, Volkman BF, Westler WM, Heckman MP, Wu JH. Solution structure of a type I dockerin domain, a novel prokaryotic, extracellular calcium-binding domain. J Mol Biol 2001;307: 745–753.
20. Lopez Garcia F, Zahn R, Riek R, Wuthrich K. NMR structure of the bovine prion protein. Proc Natl Acad Sci USA 2000;97:8334–8339.
21. Eghiaian F, Grosclaude J, Lesceu S, Debey P, Doublet B, Treguer E, Rezaei H, Knossow M. Insight into the PrPC→PrPSc conversion from the structures of antibody-bound ovine prion scrapie-susceptibility variants. Proc Natl Acad Sci USA 2004;101:10254–10259.
22. Mayer U, Kohfeldt E, Timpl R. Structural and genetic analysis of laminin-nidogen interaction. Ann NY Acad Sci 1998;857:130–142.
23. Takagi J, Yang Y, Liu JH, Wang JH, Springer TA. Complex between nidogen and laminin fragments reveals a paradigmatic beta-propeller interface. Nature 2003;424:969–974.
24. Torronen A, Rouvinen J. Structural comparison of two major endo-1,4-xylanases from *Trichoderma reesei*. Biochemistry 1995; 34:847–856.
25. Tahir TA, Berrin JG, Flatman R, Roussel A, Roepstorff P, Williamson G, Juge N. Specific characterization of substrate and inhibitor binding sites of a glycosyl hydrolase family 11 xylanase from *Aspergillus niger*. J Biol Chem 2002;277:44035–44043.
26. Payan F, Leone P, Porciero S, Furniss C, Tahir T, Williamson G, Durand A, Manzanares P, Gilbert HJ, Juge N, Roussel A. The dual nature of the wheat xylanase protein inhibitor XIP-I: structural basis for the inhibition of family 10 and family 11 xylanases. J Biol Chem 2004;279:36029–36037.
27. Velge-Roussel F, Chardes T, Mevelec P, Brillard M, Hoebeke J, Bout D. Epitopic analysis of the *Toxoplasma gondii* major surface antigen SAG1. Mol Biochem Parasitol 1994;66:31–38.
28. Sansen S, De Ranter CJ, Gebruers K, Brijs K, Courtin CM, Delcour JA, Rabijns A. Structural basis for inhibition of *Aspergillus niger* xylanase by triticum aestivum xylanase inhibitor-I. J Biol Chem 2004;279:36022–36028.
29. Schmidt A, Schlacher A, Steiner W, Schwab H, Kratky C. Structure of the xylanase from *Penicillium simplicissimum*. Protein Sci 1998;7:2081–2088.
30. Terrak M, Kerff F, Langsetmo K, Tao T, Dominguez R. Structural basis of protein phosphatase 1 regulation. Nature 2004;429:780–784.
31. Bradley P, Chivian D, Meiler J, Misura KM, Rohl CA, Schief WR, Wedemeyer WJ, Schueler-Furman O, Murphy P, Schonbrun J, Strauss CE, Baker D. Rosetta predictions in CASP5: successes, failures, and prospects for complete automation. Proteins 2003; 53(Suppl 6):457–468.
32. Gray JJ, Moughon SE, Kortemme T, Schueler-Furman O, Misura KM, Morozov AV, Baker D. Protein–protein docking predictions for the CAPRI experiment. Proteins 2003;52:118–122.
33. Schueler-Furman O, Wang C, Baker D. Progress in protein–protein docking: atomic resolution predictions in the CAPRI experiment using RosettaDock with an improved treatment of side-chain flexibility. Proteins 2005;60:187–194.